Draft version February 1, 2008
Preprint typeset using LaTeX style emulateapj v. 14/09/00

THE CONTRIBUTION OF HI-RICH GALAXIES TO THE DAMPED Ly-α ABSORBER POPULATION AT $Z = 0$

Jessica L. Rosenberg & Stephen E. Schneider
Center for Astrophysics & Space Astronomy, Department of Astrophysical and Planetary Sciences, University of Colorado, Boulder, CO 80309
Department of Astronomy, University of Massachusetts, Amherst, MA 01003
Draft version February 1, 2008

ABSTRACT

We present a study of the expected properties of the low redshift damped Ly-α absorber population determined from a sample of HI-selected galaxies in the local universe. Because of a tight correlation between the HI mass and HI cross-section, which we demonstrate spans all galaxy types, we can use our HI-selected sample to predict the properties of the absorption line systems. We use measurements of the number density and HI cross-section of galaxies to show that the total HI cross-section at column densities sufficient to produce damped Ly-α absorption is consistent with no evolution of the absorber population. We also find that the dN/dz distribution is dominated by galaxies with HI masses near 10^9 $M_\odot$. However, because of the large dispersion in the correlation between HI mass and stellar luminosity, we find that the distribution of dN/dz as a function of L_J is fairly flat. Additionally, we examine the line widths of the HI-selected galaxies and show that there may be evolution in the kinematics of HI-rich galaxies, but it is not necessary for the higher redshift population to contain a greater proportion of high mass galaxies than we find locally.

Subject headings: quasars: absorption lines — galaxies: ISM — radio lines: galaxies

1. INTRODUCTION

Damped Lyman-α absorption-line systems (DLAs) seen against background quasars are the highest column density absorbers, $N_{HI} > 2 \times 10^{20}$ cm^{-2}, and are thought to be associated with galaxies. Often they are assumed to be the disks of large spiral galaxies or their progenitors (Wolfe 1995), but there is growing evidence that not all DLAs are associated with bright spirals (e.g. Cohen 2001, Lanzetta et al. 1997, Miller et al. 1999, Colbert & Malkan 2001). The difficulty in studying the properties of these systems arises, in large part, because there are not many systems known at low-z: only 9 DLAs have been found with $z < 0.5$ (Rao & Turnshek 2000, Bowen et al. 2001a, Steidel et al. 1994, Lanzetta et al. 1997, and Le Brun et al. 1997), and only 2 of those are at $z < 0.1$ where detailed observations are possible. Absorption line studies do not provide adequate statistical samples at low-z because their pencil beams survey only small volumes of local space.

Many of the identified DLA candidates have low luminosity or low surface brightness, so it has been suggested that the absorption line population may be biased against detecting bright spiral galaxies. For example, bright spiral galaxies might contain enough dust to obscure the background QSO (Fall & Pei 1993). However, no low redshift comparison sample exists to provide an indication of what we should expect to see. In this study we construct a local comparison sample from a blind 21 cm survey we carried out at the Arecibo Observatory[1] (Rosenberg & Schneider 2001) and use it to predict the characteristics of the low redshift DLA population.

Several previous attempts have been made to predict the properties of DLAs in the local universe based on known properties of nearby galaxies. Rao & Briggs (1993) and Rao, Turnshek & Briggs (1995) combined optical luminosity functions for different morphological types with a linear relationship between HI mass and optical luminosity. They found that nearly all of the galaxy cross-section comes from large, bright spirals and that the HI cross-section implied by these galaxies would indicate a substantial decline in total HI cross-section since z=0.5. Salucci & Persic (1999) also attempted to account for the local population of DLAs by combining HI observations with optical luminosity functions. They found that large spirals contain most of the HI mass density in the local universe and that their mass density is similar to what is found in the damped absorbers. In parallel with this work, Zwaan, Briggs, & Verheijen (2001) studied a volume limited, optically selected sample of galaxies in the Ursa Major cluster. The results they obtain are similar those those found here despite concerns one may have about the optical selection and overdensity in the region.

Because galaxies with relatively high HI masses contribute most of the HI content of the local universe (Rosenberg & Schneider 2001; Zwaan et al. 1997), and because most luminous spirals have large HI masses, it may seem reasonable to conclude that luminous spirals must produce most of the absorption. The failing of this argument is that the correlation between HI mass and stellar luminosity is quite weak—a large fraction of high HI-mass systems have very low stellar luminosities, as we show in §4.2.

The recent completion of large 21 cm HI surveys provides a galaxy measurement that is more directly related to HI absorption that can be used to predict the characteristics of DLAs. Preliminary studies of these "blind" surveys (Rosenberg & Schneider 2001; Zwaan et al. 2001) suggested a significantly larger total HI cross-section for

[1] The Arecibo Observatory is part of the National Astronomy and Ionosphere Center, which is operated by Cornell University under cooperative agreement with the National Science Foundation.

the nearby galaxy population than was suggested by the earlier optically-selected samples. The present paper expands on those preliminary results with a more detailed analysis of the predicted HI and optical properties of the DLAs. In particular, we analyze near-infrared measurements of our sample of galaxies from the 2-Micron All Sky Survey (2MASS) to predict the stellar properties of the DLAs.

In Section 2 we show that an HI-selected sample makes a good basis for predicting the properties of DLAs. In addition to selecting galaxies within the same range of gas column densities, HI mass selection is nearly equivalent to selection by cross-sectional area. Section 3 contains a discussion of how dN/dz is calculated for our HI-selected sample and the resulting value of dN/dz at z=0. In Section 4 we discuss our predictions for the properties of local DLAs: HI masses (§4.1), J-band luminosities (§4.2), and kinematics (§4.3).

2. A SURROGATE SAMPLE OF DLAS IN THE LOCAL UNIVERSE

Studying the properties of damped Ly-α absorbers is difficult because it requires the systems to be nearby where absorption-line studies requires space based UV spectroscopy and the volume surveyed by each line of sight is small. To study the properties of low-z absorbers we must construct a surrogate sample for which we have better statistics. We use a blind, 21 cm emission line survey, the Arecibo Dual-Beam Survey (ADBS) as a local comparison sample for DLA properties.

The ADBS selected galaxies on the basis of their 21-cm HI flux. The survey covered ~ 430 deg^2 in the Arecibo main beam with a velocity coverage of –654 to 7977 km s^{-1} and identified 265 galaxies, with HI masses ranging from $< 2 \times 10^7$ to $> 3 \times 10^{10}$ M$_\odot$. Only a third of the ADBS galaxies had previously identified optical counterparts, partly because we detected some galaxies in the zone of avoidance, but also because there is a substantial population of low surface brightness galaxies that are not easily identified in magnitude-limited optical surveys.

To relate the ADBS detection statistics to those of DLA studies, we need to determine the cross-sectional area for the galaxies above a column density of 2×10^{20} cm^{-2}. Only a few of the ADBS sources were resolved in the Arecibo observations and, therefore, only had a measure of the total HI flux. We made spatially-resolved D-array follow-up observations from the Very Large Array[2] (VLA) for 84 of the ADBS galaxies. For this study, we use the 50 sources with a major axis diameter (at 2×10^{20} cm^{-2}) at least 40% larger than the beam to determine the HI cross-section properties of our sample.

We find that the HI cross-section is closely correlated with the HI mass of each source, as shown in Figure 1. The HI mass is determined from the source flux, distance, and linewidth using the standard equation:

$$M_{HI}/M_\odot = 2.36 \times 10^5 D^2 \int S\,dv \qquad (1)$$

where $\int S\,dv$ is the integrated line flux in Jy km s^{-1}, and D is the distance in Mpc, corrected for large scale velocity flows (Tonry et al. 2000), adopting H$_0$ = 75 km s^{-1} Mpc^{-1}. The area of the galaxy, $A_{DLA} = \pi\, a \cdot b/4$, where a and b are the major and minor axis diameters at an HI column density of 2×10^{20} cm^{-2}. The measurements for each galaxy are provided in the Appendix.

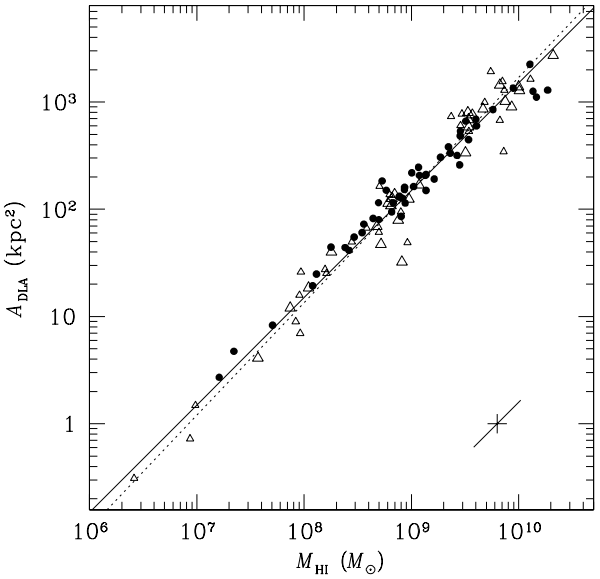

FIG. 1.— The relationship between the HI cross-section of galaxies above 2 $\times10^{20}$ cm^{-2} and HI mass. These data are from VLA D-array measurements of ADBS galaxies (solid circles) and literature values (open triangles). The galaxies marked with small triangles have minor axes at least 5 times larger than the beam while the galaxies marked with large triangles are at least 10 times larger than the beam. The ADBS sources that are included have a major axis diameter (at 2×10^{20} cm^{-2}) at least 40% larger than the beam. The error indicator at the bottom right shows the effect of ±25% distance errors (diagonal line), ±20% flux errors, and ±10% radius errors, all generous estimates of the errors.

Because most of our VLA measurements were not highly resolved, one might question whether our cross-section estimates are accurate. We have therefore consulted the literature, collecting high-resolution HI measurements for a wide variety of galaxies (see Appendix). The 53 literature sources with minor-axis dimensions at least 5 times larger than synthesized beam are shown in Figure 1 with open triangles, and are in excellent agreement with the ADBS sample, shown as solid circles. The highest-resolution literature sources (with a minor axis diameter at least 10 times larger than the beam size) are indicated by large triangles. We find no significant differences between any of these samples, leading us to conclude that the correlation seen in Figure 1 is unrelated to resolution effects. In any case, the HI masses are based on the total HI emission from the galaxy, so resolution effects could only shift points up or down in the figure and could not artificially generate the observed correlation. Distance errors *do* lead to errors parallel to the observed correlation; however, the largest conceivable errors lead to small shifts on the scale of this figure, which spans four orders of magnitude in HI mass.

We averaged forward and backward least squares fits to the high-resolution data, yielding the relationship:

$$\log(A_{DLA}) = 1.05 \cdot \log(M_{HI}) - 7.24\ , \qquad (2)$$

[2] The Very Large Array is part of the National Radio Astronomy Observatory which is a facility of the National Science Foundation operated under cooperative agreement by Associated Universities, Inc

where A_{DLA} is the cross-section in kpc^2 and M_{HI} is the HI mass in solar masses (shown in the figure by the dotted line). We find similar relationships for the ADBS data alone (although with a slope slightly less than unity), and for subsets of the high-resolution data. None of these subsets have slopes significantly different from 1. If we combine all of the data, the slope is 1.004 ± 0.021, with a correlation coefficient of 97.7%. If we assume the relationship has slope 1, the resulting fit is:

$$\log(A_{DLA}) = \log(M_{HI}) - 6.82 \ , \qquad (3)$$

and the intercept value (-6.82) is consistent for the various subsets to within ± 0.03.

A similar correlation between HI size and HI mass was previously noted for high-HI-mass galaxies by Giovanelli & Haynes (1983) using the Arecibo telescope. Their sample included galaxies in the Virgo Cluster, yet they found no significant differences between the fits for HI-deficient and HI-rich galaxies. Verheijen & Sancisi (2001) likewise observed a correlation for Ursa Major Cluster galaxies (with $M_{HI} > 10^8 M_\odot$ measuring them at a slightly lower HI column density. Our results demonstrate that the correlation spans a very wide range of masses, and the correlation is consistent whether the sample is HI-selected (ADBS galaxies) or optically selected (literature data). This indicates that the relationship between HI mass and cross-section is fundamental.

The tightness of this relationship indicates that our HI mass dependent galaxy selection is nearly equivalent to the cross-sectional area selection of the DLA population.

The strong correlation we find between HI cross-section and HI mass is probably due, in part, to measuring the galaxies at a high column density. We expect a larger dispersion at lower column densities because in the outer parts of galaxies tidal debris and gas-stripping processes have a strong effect on the measured extent. For both the ADBS and literature galaxies, the HI above the 2×10^{20} cm^{-2} isophote is generally confined to a roughly disk-shaped region, but we see emission with a wide variety of extents and morphologies at lower column densities.

Another reason for the good correlation is that the HI cross-section has a weak dependence on galaxy inclination. There is a partial cancellation between the smaller area presented by an inclined disk, and the larger radius at which the column density remains above 2×10^{20} cm^{-2} because of the longer path length through an inclined disk. We find this to be demonstrated empirically for those disk galaxies that authors have constructed inclination-corrected models of the radial dependence of HI surface density (see appendix).

Haynes & Giovanelli (1984) found a similar correlation between HI mass and the *optical* sizes of galaxies for a sample spanning a similar range in HI mass. We also find that the dimensions of ADBS galaxies as measured on the Palomar Sky Survey closely correlate with their HI mass. This suggests that the size of the optically visible region is closely related to the dense regions of the HI gas being studied here.

Finally, we note that in comparing emission and absorption line studies we are comparing gas on very different angular scales: a background quasar's extent of perhaps $0.25''$-$1''$ for absorption versus $\sim$10–$60''$ for synthesis array studies. The resolution of the synthesis data may overlook the small scale properties of these systems. If the surface filling factor for $N_{HI} > 2 \times 10^{20}$ cm^{-2} is small, we would overestimate the size of the damped region for each of these galaxies. On the other hand, there may be small regions of damped emission diluted with low column density gas beyond our measured HI isophote which contribute to a larger HI covering area. Detailed studies of the HI covering fraction are available for very few galaxies, and from what has been done to date, there are disparities in the covering fractions that have been derived. Braun & Walterbos (1992), studying the small scale HI structure in M31 with a resolution of 33 pc, find that the HI surface filling fraction approaches 1 where the emission brightness temperature exceeds $\sim$5 K (equivalent to a column density of 2×10^{20} cm^{-2} for an asymptotic temperature $T_\infty = 125$ K and a velocity width of 21.5 km s^{-1}). These numbers suggest that the correction for the covering fraction in these galaxies should be relatively small.

3. THE TOTAL CROSS-SECTION OF DLAS IN THE LOCAL UNIVERSE

We can estimate the probability of detecting a galaxy in an absorption line study if we know its cross-section and its relative contribution to the overall population of absorbers. For each ADBS galaxy we use the correlation found in the previous section to estimate its cross-section $A_{DLA}(M_{HI})$, and we determine its relative contribution based on the relative sensitivity to each source detected. We characterize the latter by the total volume $\mathcal{V}_{tot}$ within which each source could have been detected. The sensitivity criteria and completeness of the ADBS has been carefully evaluated and tested and is a function of the galaxy's flux and linewidth, the signal-to-noise ratio of the detection, and properties of the instrumental response (see Rosenberg & Schneider 2002 for a complete discussion). To find the number of systems expected per unit redshift (dN/dz), we sum over all sources:

$$dN/dz = \sum_i 1/\mathcal{V}_{tot,i} \cdot A_i(M_{HI}) \ \cdot (c/H_0) \qquad (4)$$

where $1/\mathcal{V}_{tot}$ gives the volume density for each source.

Thus, summing over all of the ADBS galaxies, our predicted total cross section at zero redshift is $dN/dz = 0.053 \pm 0.013$. We assume an error on the ADBS result of 25% as an estimate of potential systematics in the mass cross-section relationship and the covering factor to actually produce damped Ly-α absorption. The formal statistical uncertainty associated with our estimate is only a few percent.

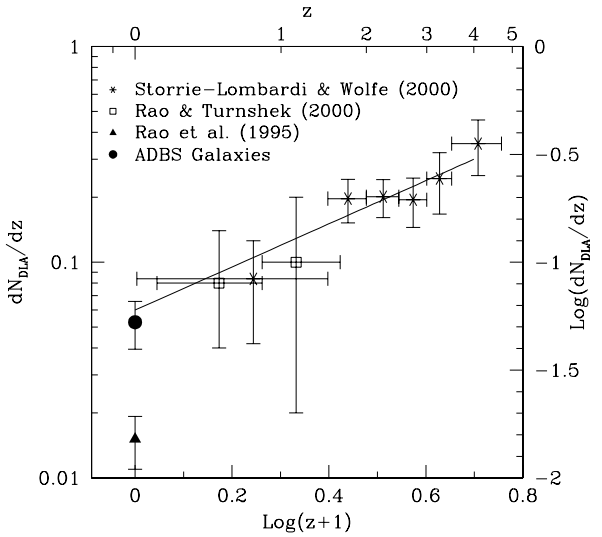

FIG. 2.— dN/dz of the DLA population as a function of redshift. The stars are from Storrie-Lombardi & Wolfe (2000), the open squares are from Rao & Turnshek (2000), the solid triangle is the $z = 0$ point from Rao et al. (1995), and the filled circle is the $z = 0$ point determined from the ADBS data in this work. The solid line is a $q_0 = 0$ no evolution model which indicates that the ADBS sample is consistent with no evolution.

Figure 2 shows dN/dz as a function of redshift for DLAs. The highest-z points, indicated by stars, are from Storrie-Lombardi & Wolfe (2000) who combined their survey of 40 quasars with previous surveys. The resulting sample contains 646 quasars and 85 DLAs with column densities $N_{HI} = 2 \times 10^{20}$ cm^{-2} covering the redshift range $0.008 < z < 4.694$. The open squares are from Rao & Turnshek (2000) whose sample consisted of 12 DLAs detected in 87 Mg II absorber lines of sight. At $z = 0$, the solid triangle is from the study of Rao et al. (1995), based on the properties of optically-selected galaxies at low redshift. The filled circle is our result described above. Our value for dN/dz at $z = 0$ is consistent with the $dN/dz(z = 0.05) = 0.08^{+0.09}_{-0.05}$ value found by Churchill (2001) for Mg II systems with strong Fe II absorption, which are good candidates for damped absorption systems (Rao & Turnshek 2000). These results are also consistent with a similar study of the HI properties of galaxies by Zwaan et al. (2001).

Our ADBS result is consistent with the $q_0 = 0$, no evolution model shown by the solid line in Figure 2. Because of the large error bars on these data, we cannot entirely rule out evolution in the DLA population. However, our result rules out strong evolution of the absorber population between $z = 0$ and $z = 0.5$ as was implied by the Rao et al. (1995) result. These results differ because the dN/dz distribution in the local universe is not dominated by large disks, but has substantial contribution from dwarf galaxies as we explore in the next section.

4. THE PREDICTED PROPERTIES OF DLAS AT $z = 0$

We have identified a sample of galaxies that we believe is representative of DLAs at $z = 0$. We use the properties of this sample to predict the nature of the DLA population locally by splitting up the contribution to dN/dz in Equation 2 according to various properties of the ADBS galaxies.

4.1. *HI Mass Distribution of DLAs*

Figure 3 shows the contribution of galaxies to dN/dz according to their HI mass. The errors for each bin have been determined from small number counting statistics using the method described by Gehrels (1986), and include no estimate of systematic errors. The vertical line indicates M_{HI_*}, the knee of the Schechter function fit to the HI mass function, as determined by Rosenberg & Schneider (2002). The dotted histogram corresponds to the determination of HI cross-section from the averaged forward and backward least squares fit, while the solid line if from the fit assuming that the slope is unity.

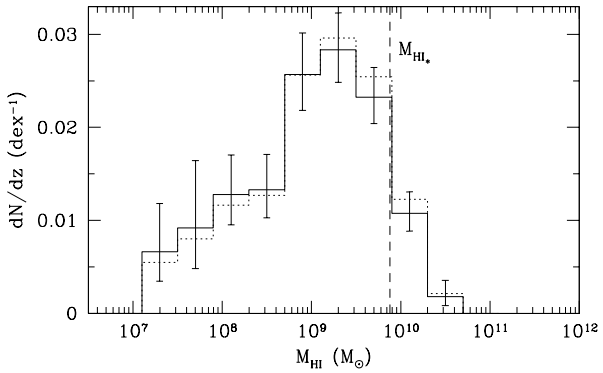

FIG. 3.— The value of dN/dz as a function of HI mass for galaxies identified in the ADBS. The errorbars represent the counting statistics errors in each bin. The figure demonstrates that most of the contribution to dN/dz comes from galaxies with HI masses near 10^9 $M_\odot$. The dashed line shows M_{HI_*}, the HI mass at the knee of the Schechter fit to the HI mass function (Rosenberg & Schneider 2002). The Milky Way contains $\sim 5 \times 10^9$ $M_\odot$ of HI (Giovanelli & Haynes 1988). The dotted line corresponds to the determination of HI cross-section from the forward and backward least squares fit, while the solid line if from the fit assuming that the slope is one.

This figure shows that the central 50% of the cross-sectional area comes from galaxies in the range $2.9 \times 10^8 < \log M_{HI}/M_\odot < 3.5 \times 10^9$. Galaxies above $M_{HI_*} = 7.6 \times 10^9$ $M_\odot$ account for only 9.5% of the area. Therefore, this central 50% of sources cover a range in HI mass from $0.04 M_{HI_*}$ to $0.46 M_{HI_*}$, relatively low HI mass sources compared to the knee of the Schechter function.

4.2. *J-Band Magnitude Distribution of DLAs*

Because L_* galaxies are a major source of the light in the universe, and M_{HI_*} galaxies are a major source of the HI mass, it is sometimes assumed that the optical counterparts to the DLAs are HI-rich L_* galaxies – bright spirals (Wolfe 1995). Instead, many of the low-z DLAs appear to be low luminosity or are not detected (Colbert & Malkan 2001, Steidel et al. 1994, LeBrun et al. 1997, Lanzetta et al. 1997, Rao & Turnshek 1998, Pettini et al. 2000). Most of the DLA candidates do not have confirmed redshifts so the actual luminosity distribution of DLAs is hard to determine. We use the ADBS sample to predict the distribution of luminosities for DLAs in the local universe by calculating the contribution to dN/dz in J-band luminosity bins.

We obtained the near infrared data used in these analyses from the 2-Micron All-Sky Survey (2MASS, Jarrett et al. 2000). 2MASS used 2 identical 1.3m telescopes in Tucson and Chile which provide simultaneous J, H, and K_s observations. Although the observing time per point is only 7.8 seconds, we were able to detect all but 27 of the galaxies in our sample on the 2MASS images. Eighteen of these were undetected while the remaining 9 did not have image data available at the time of this study. The automated 2MASS galaxy detection algorithms missed 52 faint galaxies that are visible on the images so we measured them individually within elliptical isophotes at 21 mag arcsec^{-2}. In addition, 13 galaxies had magnitudes measured by the 2MASS galaxy extraction algorithms, but for various reasons they did not have magnitudes measured at a J-band 21 mag arcsec^{-2} isophote. For the 2 galaxies which have J-band magnitudes measured within the K_s-band 20 mag arcsec^{-2} isophote, we substitute these values since these two types of magnitudes are well correlated. For the remaining 11 galaxies, we use the correlation between the J-band magnitude at 21 mag arcsec^{-2} and the magnitude in a 10″ circular aperture to calculate the magnitude. (See Rosenberg et al. 2002 for details of these galaxy measurements.)

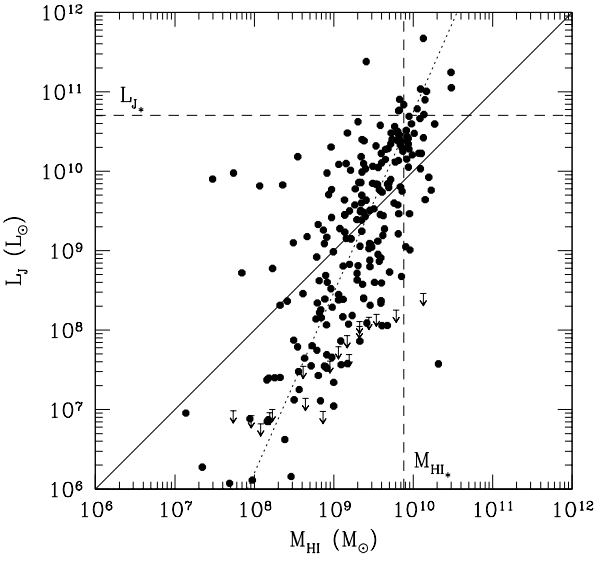

FIG. 4.— The relationship between J-band luminosity and HI mass for HI-selected galaxies (solid points). The dashed line shows the linear least squares fit to the points, and, for comparison, the solid line shows a one-to-one relationship between these quantities. The dotted lines show M_{HI_*} and L_{J_*}, the knees in the Schechter function fit.

The distribution of HI mass as a function of J-band luminosity is shown in Figure 4. The solid line in the figure shows what a one-to-one relation between L_J and M_{HI} would look like, while the dashed line shows the actual linear least-squares fit between the values ($\log(L_J) = 2.27 \log M_{HI} - 11.97$). Although there is a correlation between the the HI mass and the J-band luminosity, the relationship is nearly vertical, so that a galaxy with a given HI mass could have a J-band luminosity spanning four orders of magnitude. There is also a wide scatter in HI cross-sections for any given J-band luminosity. The dotted lines show M_{HI_*} and L_{J_*}, the knees in the Schechter function fit to, respectively, the HI mass function (Rosenberg & Schneider 2002) and J-band lumiunosity function (Kochanek et al. 2001).

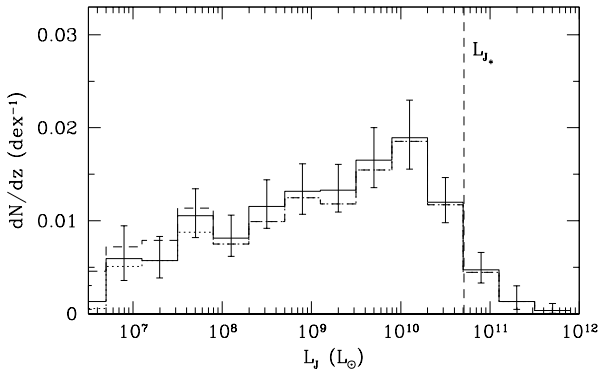

FIG. 5.— The value of dN/dz as a function of L_J. The function is very flat, indicating that there is almost uniform probability of intercepting a galaxy with a luminosity within this range along a given line of sight. Several alternative histograms are displayed to show the results for dealing with the 10% of the ADBS sample for which we had no J-band data (see text). The vertical line shows L_{J_*}, the knee in the Schechter function fit to the J-band luminosity function. The total J-band luminosity of the Milky Way is 5 $\times 10^{10} L_\odot$ (Malhotra et al. 1996).

Figure 5 shows the predicted contribution to dN/dz according to galaxy magnitude along the line of sight. The histograms assume the unity-slope fit between HI mass and cross-section (see §2), but we show several alternatives for the distribution depending on the estimates of the J-band luminosities of the undetected galaxies (see below). No matter what assumptions we make about the missing galaxies, the luminosity distribution is quite flat. Even if we make a conservative assumption that the missing galaxies are relatively bright, 50% of the galaxies lie between luminosities of $8.1 \times 10^7 L_\odot$ and $8.9 \times 10^9 L_\odot$, spanning a factor of ∼110 in luminosity. Only 4.5% of the galaxies are brighter than $J_* = -22.98$ ($L_{J_*} = 5.1 \times 10^{10} L_\odot$) (Cole et al. 2001).

In making various alternative assumptions for generating the histograms in Figure 5, we have attempted to explore what biases may have resulted from the 27 galaxies for which we have no 2MASS fluxes. The dotted-line histogram shows the result when we simply exclude the sources that were not detected. The solid-line histogram assumes that the missing galaxies had J-band luminosities determined by the fit to the mass-luminosity relation in Figure 4. This is probably an upper limit to the luminosities of the galaxies that were too faint to be detected by 2MASS. The dashed-line histogram assumes that the missing galaxies have a J-band magnitude of 19, slightly fainter than the faintest apparent magnitude we detect. The differences in the results for the 3 assumptions is small, However, if the non-detections are all very faint sources then the distribution is even flatter down to lower J-band luminosities.

The definition of "dwarf" galaxy often varies from paper to paper, but systems that are fainter than 10% of L_* are often considered dwarfs. By this definition, 63% of DLAs in the local universe should be dwarf galaxies.

4.3. *Kinematics of DLAs*

Prochaska & Wolfe (1997) argue that the kinematics of DLAs rule out the possibility that they are dwarf galaxies

at the 97% confidence level based on simulating dwarfs as slowly rotating hot disk systems. However, their definition of a dwarf is not a luminosity definition as is often used observationally, but instead is a galaxy with circular velocity less than 50 km s^{-1}. Our results above indicate that most DLAs might well be classified as dwarfs in terms of near infrared luminosity and HI mass. Significant differences between the kinematics of the low-z ADBS sample, and the $z > 1.2$ systems studied by Prochaska & Wolfe (2001, hereafter PW) could indicate evolution of the population despite the fairly constant number density of sources found above.

One complication in comparing the absorption and emission kinematics is that absorption studies probe a single line-of-sight through a galaxy's kinematic profile while emission studies probe the full extent of the system. We can make a comparison between the linewidths for the high and low redshift systems, but with the difference in the methods of measurement, we will not be able to show definitively that there has been no evolution of the population.

PW have analyzed the kinematics of 46 low-ionization lines and 32 high-ionization lines in DLAs and used them to constrain models of the origin of these systems (Prochaska & Wolfe 2001, Prochaska & Wolfe 1997; Prochaska & Wolfe 1998; Wolfe & Prochaska 2000). PW use the low-ionization transitions (Al II, Cr II, Fe II, Ni II, and Si II) as tracers of the disk component and the high-ionization transition (C IV) as a tracer of an infalling component. The velocity width of the system is defined to be 90% of the optical depth of the line. We compare our emission line widths to twice the low-ionization line widths calculated in these studies to account for the full rotation of the galaxy.

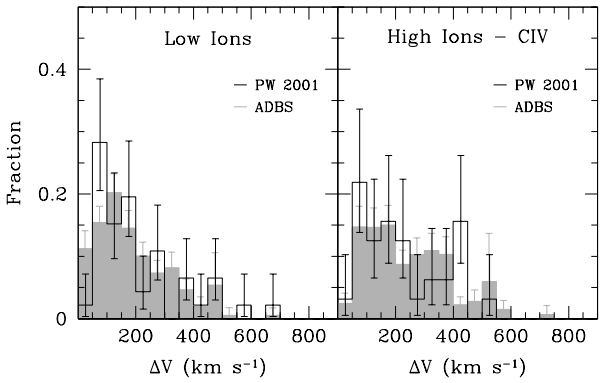

FIG. 6.— A comparison of the kinematics of the DLAs the ADBS galaxies. The figure represents the fraction of the sample in each linewidth bin. The error bars are derived from the counting statistics for each bin. The top panels show the comparison between the ADBS data (not inclination corrected; filled histograms) and twice the low ionization absorption lines widths from Prochaska & Wolfe (2001). The bottom panels shows the comparison between inclination corrected line widths from the ADBS (filled histograms) and the high ionization lines from this sample (not multiplied by two).

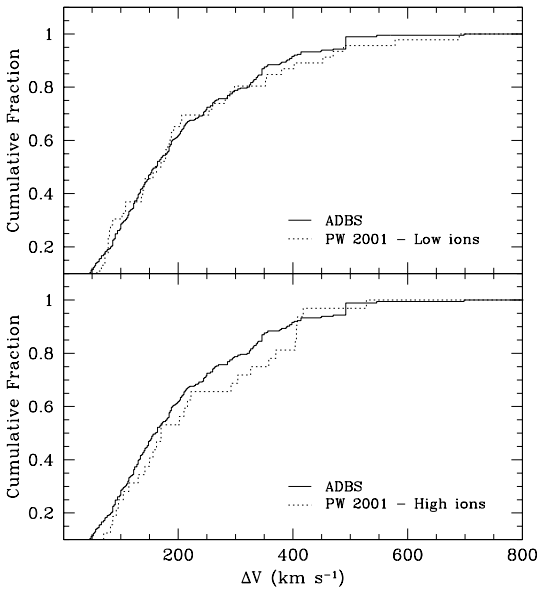

FIG. 7.— The cumulative fraction of DLAs or galaxies as a function of linewidth. The top panel shows the comparison between the ADBS data (not inclination corrected; solid histogram) and twice the low ionization absorption line widths from Prochaska & Wolfe (2001; dotted histogram). The bottom panel shows the comparison of the inclination corrected ADBS data (solid histogram) with the high ionization data (not multiplied by two) from Prochaska & Wolfe (2001; dotted histogram).

For the ADBS, we subdivide the calculated dN/dz values (§3) according to the linewidth (measured at 50% peak). The left panel in Figure 6 shows the fraction of sources with each linewidth in the ADBS sample as compared with the low-ionization species (open histograms) in the PW sample (46 DLAs). The PW widths have been multiplied by two in order to compare the single sightline velocity dispersion with the full velocity width measured by the HI. We find that the ADBS velocity widths are not significantly smaller than the DLA widths as is found for comparison with pure dwarf galaxy samples. We note that the velocity widths of the DLAs should also be corrected for the effect of only sampling a small portion of the disk, but we do not know what that correction is so we do not make it. The upper panel of Figure 7 shows the cumulative distribution comparison for the same data sets. A KS test indicates that the kinematics can be rejected as being from the same sample at the 9% confidence level. Because we do not know how to correct for the differences in disk sampling we can not show that there has been no evolution of the population, but the statistics do not require it to explain the observations.

The right panel of Figure 6 shows the comparison between the ADBS data and the high-ionization species in the PW sample (32 DLAs). Here, we have corrected the ADBS linewidths for inclination and compared then with the high-ionization lines (which have not been multiplied by two). If the high-ionization species are infalling, they should be a good probe of the galactic potential, and should measure gas from both the near and far sides of the galaxy. Here the difference between the ADBS data and the DLA data would be due to the probes not penetrating a radial line of sight through the galaxy's center. Figure 7 shows the cumulative distribution and the KS-test proba-

bility that they are drawn from different samples is 31% . There is a high line width tail for the ADBS sources that could indicate that there has been evolution, or that the absorption lines are just not probing the center of the potential.

The K-S test does not preclude that the kinematics of the ADBS galaxies and the DLAs are drawn from similar samples. It is not clear whether the kinematic differences are due to small number statistics, differences in the way the quantities are measured, or evolution of the populations. However, the ADBS line widths are, in general, as large or larger than the DLA linewidths indicating that the DLA sample does not require significantly more massive disks than those identified in an HI selected sample locally.

5. SUMMARY

We have predicted the properties of the low-z DLA population from an HI-selected galaxy survey of the local universe. The strong linear correlation between HI cross-section and HI mass means that selection effects should be very similar and allows us to use the statistics available for the properties of ADBS galaxies to predict those of low-z DLAs.

We find a much higher value of dN/dz at z=0 from the ADBS than was found for the optically-selected, spiral dominated sample of Rao et al. (1995). The Rao et al. data have been used as evidence that there was evolution of the DLA population between z=0.5 and z=0. However, the ADBS prediction for the total cross-section at $z = 0$ is consistent with dN/dz for Mg II absorbers with Fe II absorption, systems that are good candidates for damped absorption and both of these data sets indicate that no evolution is required to explain the DLA population. With the large error bars on all of the dN/dz points, we can not rule out some evolution on the DLA population, but it is not required.

The dN/dz distribution of galaxies as a function of HI mass is peaked around 10^9 $M_\odot$, and 50% of the galaxies should fall within a factor of ∼3 of this value. To date only 2 DLA absorbers have been studied in emission at 21 cm: one has a M_{HI} of 1.3 $\times 10^9$ $M_\odot$ (Bowen et al. 2001b), the other was not detected with a 3σ upper limit of 2.25 $\times 10^9$ $M_\odot$ (Kanekar et al. 2001). These results do not provide a statistical test of our HI mass distribution, but the results are consistent with what we would expect.

The ADBS sample indicates that the stellar luminosities of DLAs should be distributed fairly evenly over several orders of magnitude. As with the HI masses, there are few galaxy/DLA associations for which the galaxy redshift is confirmed and a luminosity is measured. The absorber candidates that have been identified (Steidel et al. 1994, LeBrun et al. 1997, Lanzetta et al. 1997, Rao & Turnshek 1998, Pettini et al. 2000) span a wide range of luminosities. This range of DLA luminosities is a warning for high redshift DLA candidate searches—the absorber candidates are not necessarily the nearest L_* galaxy to the line of sight.

We have compared the internal kinematics of the ADBS galaxies with those for high redshift DLAs (a low redshift sample does not exist). Prochaska & Wolfe (1997), through simulations of gas disks, rule out galaxies with small velocity widths as the primary source of damped emission at a 97% confidence level. The ADBS galaxies that we associate with the DLAs locally have larger line widths than the Prochaska & Wolfe "dwarf" galaxies, but the sample consists of a range of galaxy types dominated by galaxies with HI masses of ∼0.1 M_{HI_*} and luminosities below L_{J_*}. We find that we can not rule out evolution in the kinematics of HI-rich galaxies, but it is not required and more massive HI disks then found in our local sample are not necessary to account for the kinematics.

We thank Jason X. Prochaska for helpful discussions about the kinematics of DLAs and the referee for a thoughtful reading of this paper. We would also like to thank the VLA staff for their assistance in the observations and reduction of this data, and the 2MASS team for all of the hard work that went into making the survey a reality.

APPENDIX

APPENDIX

In this appendix we present VLA data for the ADBS sample of galaxies, as well as high-resolution literature data used as a comparison sample to confirm our results. In addition, we provide some further analysis of the HI cross-sections of the galaxies beyond the analysis in the main text.

VLA HI Data for the ADBS

The galaxies in the ADBS were observed with the VLA in D-array, with relatively short duration (10 to 15 min) integrations. These were usually split into two time intervals in order to improve the u-v coverage of the observations. Further details of the observational procedures can be found in Rosenberg & Schneider (2002).

We present the basic information on the 50 sources detected with the VLA that have a major axis diameter (at 2×10^{20} cm^{-2}) at least 40% larger than the beam.. All were reduced using the observatory's *AIPS* routine *IMAGR*, setting the *ROBUST* parameter to 0. This provides a good compromise, providing nearly as good noise characteristics as natural weighting and nearly as small a beam as uniform weighting. Table A.1 lists the FWHM dimensions of the beam along with other measured parameters for the galaxies.

The elliptical dimensions of the galaxies at a column density of 2×10^{20} cm^{-2} were fit to the total HI maps using the *IRAF STSDAS* package *ELLIPSE*. The mean velocities and total HI masses determined from the VLA observations are all consistent with our Arecibo detection measurements. We also provide a flow-corrected distance estimate based on Tonry et al. (2000), assuming $H_0 = 75$ km s^{-1} Mpc^{-1}.

HI Synthesis Data from the Literature

We compiled higher-resolution HI measurements from the literature for comparison with our results. We consulted sources listed in Martin's (1998) bibliographic compilation of HI maps in order to identify synthesis observations with beam sizes at least ten times smaller than the reported HI dimensions. We further restricted our sample to sources that Martin indicated reached column densities below 2×10^{20} cm^{-2} and which had both HI contour maps and radial density profiles. This yielded about 100 candidate sources. We found that the resulting list contained few low-mass sources, so we added several more-recent papers that concentrated on dwarf galaxies. The resulting sample spans all galaxy types from giant ellipticals to dwarf irregulars.

Table A.2 compiles the information collected from these papers in a similar format as for our ADBS galaxies. None of the papers directly reported the dimensions of the galaxy at 2×10^{20} cm^{-2}, so we estimated them from the HI column density contour maps. The beam dimensions are those reported in each paper for the contour maps. In a few cases (noted by the word "ring" or "mult" in the notes column of the table) the distribution of HI above 2×10^{20} cm^{-2} was not well described as a disk. In these cases, we give major and minor axis dimensions that approximately indicate (a) the combined length of the regions of HI that exceeded our fiducial level, and (b) the narrower dimension of these regions. These dimensions should yield a fairly accurate total cross-section for the sources. We note that many other sources also showed irregularities around the edges, or small holes or small regions outside the main disk, but these amount to only slight deviations in the overall dimensions of the sources.

For papers that displayed inclination-corrected, azimuthally-averaged radial density profiles, we again used the published plots to estimate the radius at which the HI column density reached our fiducial level. In a few cases the radial profile was plotted, but did not exceed the 2×10^{20} cm^{-2} level. In all of these cases, the HI contour map had regions above this level, but the azimuthal averaging had produced a lower mean level. We note that these radial profiles are quite sensitive to the inclination estimates. As a result, they tend to be more accurate for disk galaxies, and much less so for dwarf irregulars.

The redshifts and morphological types listed in the table were taken from the NASA/IPAC Extragalactic Database (NED). The distances are again based on the flow-corrected Tonry model, except when the redshift was less than 250 km s^{-1}, in which case we used the distance quoted by the author. For two of these nearby galaxies, UGC 8091 (Dohm-Palmer et al. 1998) and UGC 12613 (Gallagher et al. 1998), recent distance estimates were significantly different from those reported in the HI paper, and we have adopted the newer values.

The HI Mass/Cross-Section Correlation

The strong, one-to-one correlation between HI mass and cross-section over such a wide range of galaxy sizes and masses is somewhat surprising. At first glance, it suggests that all types of galaxies share the same surface density of HI. Actually the data are a little more complicated to interpret, since the relationship is between the total HI, and the area of the disk that exceeds the relatively high surface density of 2×10^{20} cm^{-2}. If all galaxies had their HI in exponential disks with varying scale lengths but the same central surface brightness, such a relationship would pertain, but clearly that is not a realistic description of galaxy HI distributions. We present here a few exploratory comments about the data presented in Table A.2 to examine this correlation in greater detail.

For the central purpose of this paper, we focused on the relationship between the HI mass and the *observed* cross-section of HI on the sky. However, as we briefly noted in §2, the observed cross-section is relatively independent of inclination. We show this in Figure A8, where we plot the ratio of observed to face-on cross sections above 2×10^{20} cm^{-2} as a function of the observed axis ratio. The sample shown is the subset of galaxies from Figure 1 that also had inclination-corrected radial profile models. The cross-section does not simply decline as $\cos(i)$ (curve in figure), as would occur for a sharp-edged disk. Because of the longer path length through the disk, the 2×10^{20} cm^{-2} isophote shifts outward to a physically larger radius by an amount that depends on the scale-length of the HI distribution. The two effects nearly cancel for most inclinations, although edge-on galaxies do finally exhibit a significantly smaller cross-section. Overall, the observed cross-sections are about 25% smaller, on average, than the inclination-corrected models predict for galaxies with axis ratios larger than $b_{DLA}/a_{DLA} > 0.5$.

The scatter about the fit between mass and cross-sectional area improves slightly when we use azimuthally-averaged, inclination-corrected model results. Using these face-on cross-sections yields a similar slope (1.04 ± 0.04) as we found using the observed cross-sections in a linear least squares fit, although the intercept shifts because of the larger cross-section found on average for the face-on models. We will assume both actually have slope unity so that we can just compare the distribution of $\log[M_{HI}/A_{DLA}]$. For the 64 galaxies with measurements of both the face-on, a_0, and observed dimensions, $a_{DLA} \times b_{DLA}$, the rms scatter of $\log[M_{HI}/A_{DLA}]$ is 0.194 and 0.227 respectively.

There seems to be little dependence with morphological type. If we use observed cross-sections for galaxies which are not highly inclined ($b_{DLA}/a_{DLA} > 0.5$), we find the following results by morphological type:

Type	N	$\log[M_{HI}/A_{DLA}]$
Sa – Sb	10	6.71 ± 0.08
Sbc – Sd	14	6.85 ± 0.03
Sdm – Im	15	6.77 ± 0.04

The earliest-type galaxies (Sa – Sb) may have slightly lower values of $\log[M_{HI}/A_{DLA}]$ than late-types, but the difference is marginal. This appears to be true for the S0's as well, but our few examples have peculiar HI distributions, so any

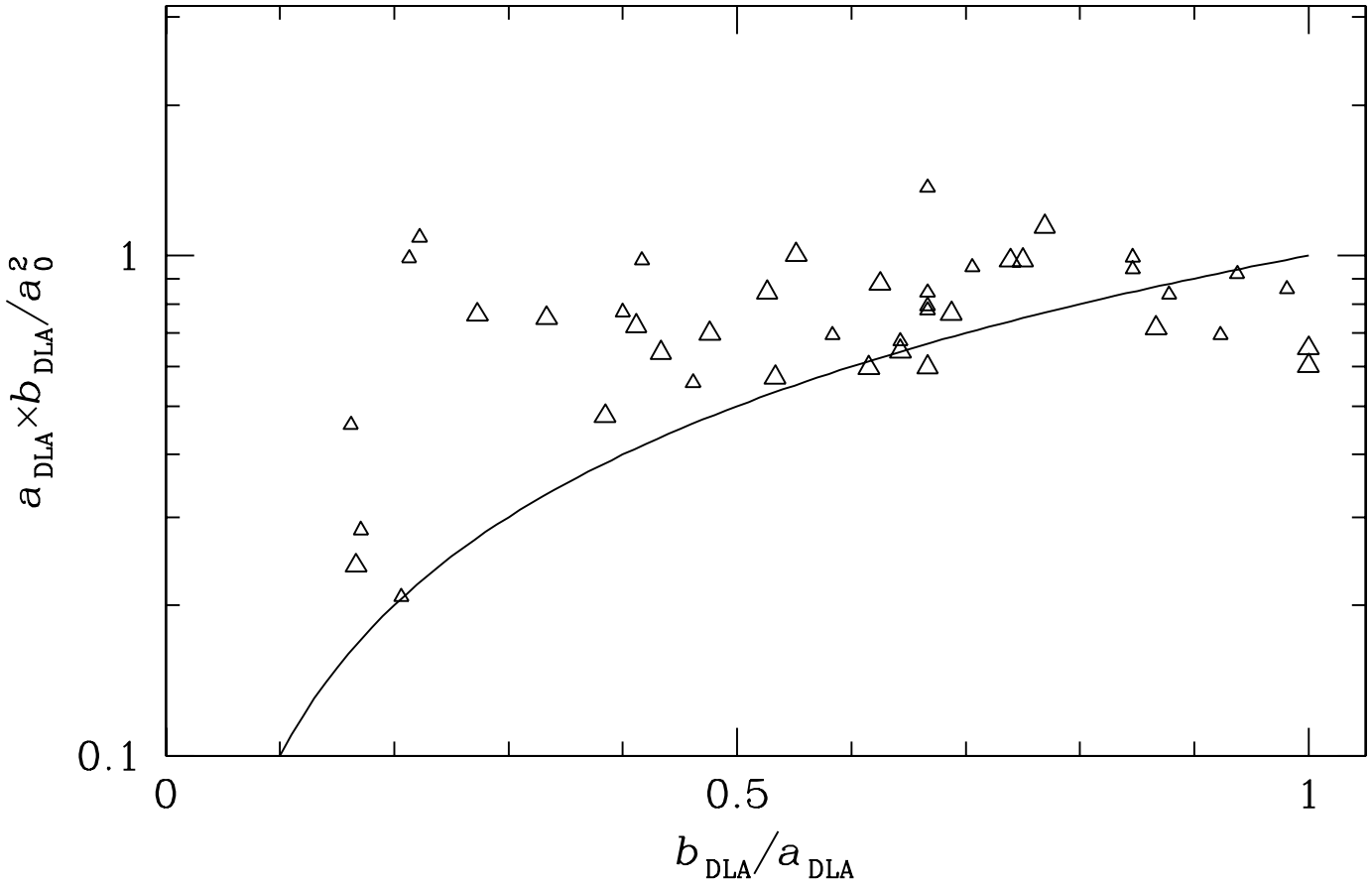

FIG. A8.— The ratio of the observed cross-section to the predicted face-on cross-section as a function of observed axis ratio. The galaxies marked with small triangles have minor axes at least 5 times larger then the beam while the galaxies marked with large triangles are at least 10 times larger than the beam. The curve shows the expected ratio if the cross-section varied as $\cos(i)$.

conclusions depend on whether the model or observed cross-sections are used, and whether outliers are rejected. While there may be some dependence on morphological type, the remarkable thing is how little variability there is between types over an enormous range of masses.

TABLE A.1
HI SIZES AT $N_{HI} = 2 \times 10^{20}$ FROM THE ADBS

Name	D_{beam} [′]	D [′]	V_{hel}	Dist. [Mpc]	$\log(M_{HI})$ [$M_\odot$]
002526+2136	0.95×0.70	1.5×1.1	5001	66.7	9.44
014729+2719	0.87×0.81	7.8×2.9	743	9.9	9.14
015434+2312	0.98×0.87	1.5×1.4	5298	70.6	9.60
020320+1837	0.90×0.83	2.8×2.7	2727	36.4	9.50
020320+2345	0.88×0.82	1.5×1.4	3081	41.1	9.06
020405+2412	0.95×0.85	1.5×1.5	989	13.2	8.11
022859+2808	0.87×0.82	2.5×1.5	1341	17.9	8.69
023323+2810	0.87×0.82	1.8×1.2	1316	17.5	8.23
023622+2526	0.88×0.83	9.6×2.3	987	13.2	9.45
025537+1938	0.95×0.87	3.1×1.5	893	11.9	8.38
025726+1008	0.94×0.86	3.0×1.7	1092	14.6	8.56
030546+2212	0.96×0.87	3.1×1.9	4365	58.2	9.94
031420+2409	0.88×0.84	3.9×1.9	1523	20.3	9.12
040344+2209	0.99×0.90	2.2×2.2	6307	84.1	10.09
040411+2207	0.97×0.87	1.8×1.5	6320	84.3	10.13
053017+2233	0.92×0.83	1.5×1.0	2555	34.1	8.64
055517+2526	0.90×0.84	1.8×1.6	1547	20.6	8.64
062054+2008	1.10×0.89	3.7×1.8	1279	17.1	8.86
065406+0834	1.21×0.93	2.6×1.8	2420	32.3	9.42
070920+2038	1.09×0.90	2.6×1.8	4879	65.1	10.27
071225+2342	1.12×0.89	2.3×1.9	4138	55.2	9.76
071352+1031	1.02×0.81	3.6×2.1	304	4.1	7.69
071553+1207	1.04×0.84	2.4×2.0	1972	26.3	8.98
081726+2110	1.22×0.89	1.8×1.7	2036	27.1	8.92
090024+2536	1.27×0.87	3.8×2.3	1806	24.1	9.36
090526+2533	1.09×0.88	2.6×2.1	2869	38.3	9.44
101421+2207	1.05×0.86	1.5×1.2	1686	22.5	8.49
103143+2518	1.22×0.86	3.7×2.6	1205	16.1	9.00
103439+2305	1.20×0.85	2.1×1.7	1142	15.2	8.46
104722+1404	1.10×0.84	2.5×2.3	264	3.5	7.34
104916+1226	1.39×0.90	4.1×2.5	1238	16.5	8.73
110710+1834	1.29×0.87	4.0×2.1	1082	14.4	8.94
112914+2035	1.01×0.85	2.1×2.0	1392	18.6	8.82
115004+2628	1.09×0.86	2.0×1.8	2096	27.9	9.21
115040+2531	1.07×0.86	2.3×1.3	2149	28.7	8.91
120033+2004	1.04×0.85	3.9×2.9	1254	16.7	9.14
121516+2038	1.04×0.85	5.0×4.1	743	9.9	8.89
123606+2602	1.51×0.85	15.0×3.0	1453	19.4	10.17
124516+2708	1.66×0.86	3.0×2.2	1050	14.0	8.87
125223+2138	1.29×0.87	3.1×2.3	479	6.4	8.08
131652+1232	1.09×0.85	3.3×2.2	689	9.2	8.41
141556+2303	0.93×0.85	2.7×2.2	195	2.6	7.21
144842+1226	1.18×0.84	3.3×2.6	1950	26.0	9.35
145647+0930	1.35×0.84	2.4×2.0	3221	42.9	9.59
154540+2805	1.09×0.86	2.4×1.9	2353	31.4	9.27
163122+2010	1.28×0.85	3.5×1.6	2560	34.1	9.53
214731+2209	0.99×0.84	1.9×1.4	2033	27.1	8.90
214813+2209	1.00×0.84	2.3×2.0	1967	26.2	9.06
225557+2610	0.96×0.84	1.4×1.1	2979	39.7	8.72
230433+2709	0.96×0.85	3.0×1.6	1439	19.2	8.82

TABLE A.2
HI SIZES AT $N_{HI} = 2 \times 10^{20}$ FROM THE LITERATURE

Name	D_{beam} [′]	D [′]	D_{corr} [′]	V_{hel}	Dist. [Mpc]	$\log(M_{HI})$ [$M_\odot$]	Type	Morph.	Reference
NGC 55	0.75×0.75	41.0×7.0	31.9	129	1.6	8.96	SB(s)m:	···	Puche et al. (1991)
NGC 247	0.75×0.75	37.0×6.0	22.0	160	2.5	8.90	SAB(s)d	···	Carignan & Puche (1990b)
NGC 300	0.83×0.83	32.0×20.0	27.0	144	1.8	8.84	SA(s)d	···	Puche et al. (1990)
IC 1613	2.00×2.00	22.0×4.0	···	-234	0.7	7.78	IB(s)m	ring	Lake & Skillman (1989)
UGC 891	0.64×0.56	4.5×1.7	5.1	643	14.6	9.11	SABm:	···	van Zee et al. (1997)
M 74	0.80×0.39	15.0×13.0	16.5	657	14.5	10.32	SA(s)c	···	Wevers et al. (1986)
UGCA 20	0.18×0.18	4.5×1.5	···	498	12.2	8.58	Im	mult	van Zee et al. (1996)
NGC 925	0.77×0.42	12.0×8.0	12.7	553	11.9	9.93	SAB(s)d	···	Wevers et al. (1986)
NGC 1058	0.72×0.70	10.5×7.0	7.3	518	11.1	9.46	SA(rs)c	···	Dickey et al. (1990)
NGC 1073	0.34×0.33	7.0×7.0	8.7	1211	21.0	9.82	SB(rs)c	···	England et al. (1990)
UGC 2259	0.37×0.37	4.1×3.6	4.2	583	11.8	8.80	SB(s)dm	···	Carignan et al. (1988)
NGC 1140	0.62×0.50	7.7×3.0	4.7	1501	25.1	9.72	IBm:	···	Hunter et al. (1994)
NGC 1291	0.80×0.80	8.5×2.5	···	839	15.5	9.41	(R)SB(l)0/a	ring	van Driel et al. (1988b)
NGC 1300	0.33×0.33	7.0×4.5	7.0	1568	25.7	10.00	(R')SB(s)bc	···	England (1989)
UGC 2684	0.50×0.48	3.5×1.4	3.1	350	8.9	8.38	Im?	···	van Zee et al. (1997)
NGC 1343	1.17×0.78	6.3×4.9	···	2215	31.1	9.72	SAB(s)b:	···	Taylor et al. (1994)
NGC 1398	0.99×0.96	9.0×6.0	8.3	1407	23.2	9.74	(R')SB(rs)ab	···	Moore & Gottesman (1995)
IC 342	2.00×1.90	60.0×50.0	52.0	31	2.0	9.53	SAB(rs)cd	···	Newton (1980)
NGC 1560	0.23×0.22	18.0×3.0	15.0	-36	3.0	8.91	SA(s)d	···	Broeils (1992)
UGC 3174	0.72×0.62	4.8×2.4	4.1	670	10.9	8.60	IAB(s)m:	···	van Zee et al. (1997)
UGCA 116	0.14×0.13	6.1×1.3	2.8	789	10.8	8.70	BCD/Sbc	mult	van Zee et al. (1998)
NGC 2366	0.43×0.42	13.0×5.0	11.7	100	3.3	8.72	IB(s)m	···	Wevers et al. (1986)
NGC 2403	0.75×0.75	30.0×16.0	29.0	131	3.2	9.51	SAB(s)cd	···	Wevers et al. (1986)
UGC 3974	0.13×0.12	8.0×6.0	7.0	272	3.5	8.25	IB(s)m	···	Walter & Brinks (2001)
UGC 4483	0.18×0.15	2.6×2.0	2.1	178	3.4	7.57	Dwarf	···	van Zee et al. (1998)
NGC 2787	0.45×0.42	6.0×1.0	···	696	10.9	8.73	SB(r)0+	ring	Shostak (1987)
NGC 2841	1.08×0.85	27.0×6.0	12.2	638	8.3	9.37	SA(r)b:	···	Bosma (1981)
NGC 2903	0.55×0.55	17.0×7.0	12.8	556	4.6	9.07	SB(s)d	···	Wevers et al. (1986)
Holmberg I	0.20×0.18	5.0×4.3	···	143	3.6	8.04	IAB(s)m	···	Ott et al. (2001)
Leo A	0.38×0.38	8.7×4.3	···	20	2.2	7.87	IBm	···	Young & Lo (1996)
NGC 3079	0.29×0.25	9.7×2.0	9.7	1125	16.4	9.86	SB(s)c	···	Irwin & Seaquist (1991)
NGC 3198	0.58×0.42	21.0×7.0	14.0	663	7.7	9.53	SB(rs)c	···	Begeman (1989)
IC 2574	0.50×0.50	19.0×10.0	15.0	57	3.0	8.78	SAB(s)m	···	Martinbeau et al. (1994)
UGC 5716	0.54×0.53	3.5×2.3	3.1	1277	16.3	8.76	Sm:	···	van Zee et al. (1997)
UGC 5764	0.53×0.50	3.8×1.8	3.0	586	5.0	7.79	IB(s)m:	···	van Zee et al. (1997)
UGC 5829	0.33×0.33	6.0×5.3	···	629	5.7	8.68	Im	···	Taylor et al. (1994)
KDG 73	0.20×0.17	1.6×0.5	···	113	3.6	6.32	Im	mult	Ott et al. (2002)
NGC 3510	1.03×0.95	6.5×2.0	···	705	5.9	8.59	SB(s)m	···	Taylor et al. (1994)
NGC 3626	0.68×0.22	8.0×0.8	···	1493	19.7	8.89	(R)SA(rs)0+	mult	van Driel et al. (1989)
NGC 3628	0.50×0.50	12.0×2.1	10.1	843	6.2	9.38	SAb:	···	Wilding et al. (1993)
NGC 3726	0.63×0.47	12.0×5.0	7.8	866	11.6	9.54	SAB(r)c	···	Wevers et al. (1986)
UGC 6578	0.17×0.14	1.3×1.1	1.2	1099	9.7	7.92	pair	···	van Zee et al. (1998)

TABLE A.2—*Continued*

Name	D_{beam} [′]	D [′]	D_{corr} [′]	V_{hel}	Dist. [Mpc]	$\log(M_{HI})$ [$M_\odot$]	Type	Morph.	Reference
NGC 3900	0.90×0.42	5.2×2.4	5.8	1798	28.5	9.50	SA(r)0+	···	van Driel et al. (1989)
UM 461	0.18×0.16	2.4×1.6	2.1	1039	7.9	7.96	BCD/Irr	···	van Zee et al. (1998)
UGC 6850	0.17×0.14	1.3×1.2	1.5	1055	8.2	7.96	Pec	···	van Zee et al. (1998)
NGC 3941	0.67×0.42	7.0×1.5	···	928	11.7	8.76	$SB(s)0^0$	ring	van Driel & van Woerden (1989)
M 109	0.44×0.33	10.5×5.0	8.7	1048	15.7	9.67	SB(rs)bc	···	Gottesman et al. (1984)
NGC 4151	0.36×0.29	7.5×7.5	9.7	995	13.5	9.53	(R')SAB(rs)ab:	···	Pedlar et al. (1992)
UGC 7178	0.57×0.53	3.2×3.0	3.2	1339	16.0	8.70	IAB(rs)m:	···	van Zee et al. (1997)
M 98	1.17×0.80	13.5×3.0	7.0	-142	17.0	9.72	SAB(s)ab	···	Cayatte et al. (1990)
NGC 4216	0.80×0.78	7.0×1.7	5.5	131	17.0	9.35	SAB(s)b:	···	Cayatte et al. (1990)
NGC 4222	0.80×0.78	4.5×1.5	···	230	17.0	8.95	Sc	···	Cayatte et al. (1990)
NGC 4242	0.58×0.42	6.0×4.0	5.5	517	5.6	8.44	SAB(s)dm	···	Wevers et al. (1986)
M 99	1.08×0.70	7.5×5.0	6.3	2407	34.6	10.33	SA(s)c	···	Cayatte et al. (1990)
M 61	0.75×0.73	8.5×6.0	7.3	1566	19.5	9.87	SAB(rs)bc	···	Cayatte et al. (1990)
M 100	0.75×0.70	6.5×5.5	6.0	1571	20.4	9.68	SAB(s)bc	···	Cayatte et al. (1990)
NGC 4395	0.80×0.43	16.0×11.0	15.2	319	3.0	8.81	SA(s)m:	···	Wevers et al. (1986)
NGC 4402	0.35×0.28	2.1×0.6	1.8	232	17.0	8.68	Sb	···	Cayatte et al. (1990)
M 88	0.67×0.65	6.5×2.5	4.7	2281	33.4	9.82	SA(rs)b	···	Cayatte et al. (1990)
NGC 4535	0.70×0.68	7.0×4.5	6.8	1961	27.9	10.11	SAB(s)c	···	Cayatte et al. (1990)
IC 3522	0.40×0.40	3.0×2.1	···	668	8.1	8.19	ImIII-IV	···	Skillman et al. (1987)
NGC 4568	0.67×0.67	4.0×2.5	···	2255	33.5	9.50	SA(rs)bc	···	Cayatte et al. (1990)
M 58	0.32×0.30	3.5×1.0	4.0	1519	19.6	8.88	SAB(rs)b	mult	Cayatte et al. (1990)
NGC 4654	0.80×0.72	5.5×3.5	5.3	1037	13.3	9.33	SAB(rs)cd	···	Cayatte et al. (1990)
UGC 7906	0.40×0.40	2.4×1.1	···	1010	12.7	8.19	ImIV	···	Skillman et al. (1987)
NGC 4725	0.97×0.42	12.0×7.0	11.0	1206	16.7	9.85	SAB(r)ab	···	Wevers et al. (1986)
M 94	0.83×0.83	4.6×3.3	5.7	308	3.5	8.43	(R)SA(r)ab	···	Mulder & van Driel (1993)
NGC 4731	0.55×0.38	8.5×6.0	···	1495	17.3	9.87	SB(s)cd	···	Gottesman et al. (1984)
NGC 4789A	0.75×0.75	10.0×4.0	7.2	374	3.1	8.21	IB(s)mIV-V	···	Carignan & Beaulieu (1989)
UGC 8091	0.29×0.29	2.2×2.1	···	214	2.2	6.99	ImV	···	Lo et al. (1993)
NGC 5033	0.72×0.43	13.0×6.0	11.8	875	11.4	9.83	SA(s)c	···	Wevers et al. (1986)
M 63	1.22×0.82	30.0×13.0	24.7	504	5.4	9.57	SA(rs)bc	···	Bosma (1981)
UGC 8333	0.40×0.33	4.6×1.4	···	935	11.3	8.60	Im:	···	Lake et al. (1990)
NGC 5101	0.67×0.67	6.5×1.5	6.8	1861	20.3	9.48	(R')SB(rl)0/a	ring	van Driel et al. (1988b)
NGC 5102	0.62×0.57	11.0×4.5	···	467	2.8	7.97	SA0-	···	van Woerden et al. (1993)
NGC 5371	0.72×0.47	6.0×3.0	4.3	2553	38.9	9.97	SAB(rs)bc	···	Wevers et al. (1986)
NGC 5585	0.52×0.52	11.6×6.4	8.6	305	5.0	8.98	SAB(s)d	···	Cote et al. (1991)
NGC 6503	0.43×0.42	22.0×6.0	13.2	60	3.8	8.82	SA(s)cd	···	Wevers et al. (1986)
ESO 594-G004	0.37×0.25	4.1×2.2	···	-77	1.1	6.94	IB(s)m:	mult	Young & Lo (1997)
NGC 6814	0.86×0.70	5.3×5.2	5.7	1563	20.6	9.47	SAB(rs)bc	···	Liszt & Dickey (1995)
NGC 6946	0.67×0.62	23.0×17.0	20.0	48	7.0	10.01	SAB(rs)cd	···	Tacconi & Young (1986)
UGC 11820	0.73×0.59	4.9×2.9	5.2	1104	18.7	9.50	Sm	···	van Zee et al. (1997)
NGC 7331	0.75×0.42	15.0×3.5	13.6	816	15.8	10.02	SA(s)b	···	Bosma (1981)
IC 5267	0.67×0.67	13.0×1.4	1.7	1713	27.5	9.63	(R)SA(rs)0/a	ring	van Driel et al. (1988b)

TABLE A.2—*Continued*

Name	D_{beam} [′]	D [′]	D_{corr} [′]	V_{hel}	Dist. [Mpc]	$\log(M_{HI})$ [$M_\odot$]	Type	Morph.	Reference
UGC 12613	0.24×0.24	4.5×1.8	···	-183	0.8	6.42	dIrr/dSph	···	Lo et al. (1993)
NGC 7793	0.75×0.75	13.0×8.0	13.2	230	3.4	8.88	SA(s)d	···	Carignan & Puche (1990a)

REFERENCES

Begeman, J. H. 1989, A&A, 223, 47.
Bosma, A. 1981a, AJ 86, 1791.
Bosma, A. 1981b, AJ 86, 1825.
Bowen, D. V., Tripp, T. M., & Jenkins, E. B. 2001a, AJ, 121, 1456.
Bowen, D. V., Huchtmeier, W., Brinks, E., Tripp, T. M., Jenkins, E. B. 2001b, A & A, 372, 820.
Braun, R. & Walterbos, R. A. M. 1992, ApJ, 386, 120.
Broeils, A. H. 1992, A&A, 256, 19.
Carignan, C., & Beaulieu, S. 1989, ApJ, 347, 760.
Carignan, C., & Puche, D. 1990a, AJ, 100, 394.
Carignan, C., & Puche, D. 1990b, AJ, 100, 641.
Carignan, C., Sancisi, R., & van Albada, T.S. 1988, AJ, 95, 37.
Cayatte, V., van Gorkom, J. H., Balkowski, C., & Kotanyi, C., 1990, AJ, 100, 604.
Churchill, C. W. 2001, ApJ, 560, 92.
Cohen, J. G. 2001, ApJ, 121, 1275.
Colbert, J. W. & Malkan, M. A. 2001, astro-ph/0112416.
Cole, S., Norberg, P., Baugh, C. M., Frenk, C. S., Bland-Hawthorn, J., Bridges, T., Cannon, R., Colless, M., Collins, C., Couch, W., Cross, N., Dalton, G., De Propris, R., Driver, S. P., Efstathiou, G., Ellis, R. S., Glazebrook, K., Jackson, C., Lahav, O., Lewis, I., Lumsden, S., Maddox, S., Madgwick, D., Peacock, J. A., Peterson, B. A., Sutherland, W., Taylor, K. 2001, MNRAS, 326, 255.
Coté, S., Carignan, C., & Sancisi, R. 1991, AJ, 102, 904.
Dickey, J. M., Murray-Hanson, M., & Helou, G. 1990, ApJ, 352, 522.
England, M. N. 1989, ApJ, 337, 191.
England, M. N., Gottesman, S. T., & Hunter Jr., J. H. 1990, ApJ, 348, 456.
Fall, S. M. & Pei, Y. C. 1993, ApJ, 402, 479.
Gehrels, N. 1986, ApJ, 303, 336.
Giovanelli, R. & Haynes, M. P. 1988, in Galactic and Extragalactic Radio Astronomy, eds. G. L. Verschuur and K. I. Kellerman, Springer Verlag: New York.
Giovanelli, R. & Haynes, M. P. 1983, ApJ, 88, 881.
Gottesman S. T., Ball R., Hunter Jr. J. H., & Huntley J.M. 1984, ApJ, 286, 471
Haynes, M. P. & Giovanelli, R. 1984, ApJ, 89, 758.
Hunter, D. A., van Woerden, H., & Gallagher III, J. S., 1994, ApJS, 91, 79 Irwin, J. A., & Seaquist, E. R. 1991, ApJ, 371, 111
Jarrett, T. H., Chester, T., Cutri, R., Schneider, S., Skrutskie, M., Huchra, J. P. 2000, AJ, 119, 2498.
Kanekar, N., Chengalur, J. N., Subramanyan, R., & Petitjean, P. 2001, A & A, 367, 46.
Kochanek, C. S., Pahre, M. A., Falco, E. E., Huchra, J. P., Mader, J., Jarrett, T. J., Chester, T., Cutri, R., & Schneider, S. E. 2001 ApJ, 560, 566.
Lake, G., Schommer, R. A., & van Gorkom, J.H. 1990, AJ, 99, 547.
Lake, G., & Skillman, E.D. 1989, AJ, 98, 1274.
Lanzetta, K. M., Wolfe, A. M., Altan, H., Barcons, X., Chen, H.-W., Fernandez-Soto, A., Meyer, D. M., Ortiz-Gil, A., Savaglio, S., Webb, J. K., & Yahata, N. 1997, AJ, 114, 1337.
Le Brun, V., Bergeron, J., Boisse, P., & Deharveng, J. M. 1997, A & AS, 321, 733.
Ledoux, C., Petitjean, P., Bergeron, J., Wampler, E. J., & Srianand, R. 1998, A & A, 337, 51.
Liszt, H. S., & Dickey, J. M. 1995, AJ, 110, 998.
Lo, K. Y., Sargent, W. L. W., & Young, K. 1993, AJ, 106, 507.
Malhotra, S., Spergel, D. N., Rhoads, J. E., & Li, J. 1996, ApJ, 473, 687.
Martimbeau, N., Carignan, C., & Roy, J. R. 1994, AJ, 107, 543.
Martin, M. C. 1998, A&AS, 131, 73.
Miller, E. D., Knezek, P. M., & Bregman, J. N. 1999, ApJ, 510, L95.
Moore, E. M., & Gottesman, S. T. 1995, ApJ, 447, 159.
Mulder, P. S., & van Driel, W. 1993, A&A, 272, 63.
Newton, K. 1980, MNRAS, 191, 615.
Ott, J., et al. 2002, in preparation.
Ott, J., Walter, F., Brinks, E., Van Dyk, S. D., Dirsch, B., & Klein, U. 2001, AJ, 122, 3070.
Pedlar, A., Howley, P., Axon, D. J., & Unger, S. W. 1992, 259, 369.
Pettini, M., Ellison, S. L., Steidel, C. C., Shapley, A. E., & Bowen, D. V. 2000, ApJ, 532, 65.
Prochaska, J. X. & Wolfe, A. M. 1997, ApJ, 487, 73.
Prochaska, J. X. & Wolfe, A. M. 1998, ApJ, 507, 113.
Puche, D., Carignan, C., & Bosma, A. 1990, 100, 1468.
Puche, D., Carignan, C., & Wainscoat, R. J. 1991, AJ, 101, 447.
Rao, S. M., & Briggs, F. H. 1993, ApJ, 419, 515.
Rao, S. M. & Turnshek, D. A. 2000, ApJS, 130, 1.
Rao, S. M. & Turnshek, D. A. 1998, ApJ, 500, 115.
Rao, S. M., Turnshek, D. A., & Briggs, F. H. 1995, ApJ, 449, 488.
Rosenberg, J. L. & Schneider, S. E. 2001, in Extragalactic Gas at Low Redshift, ed. J. S. Mulchaey & J. Stocke (San Francisco: ASP), 254, 179.
Rosenberg, J. L. & Schneider, S. E. 2002, ApJ, 568, 1.
Rosenberg, J. L., Schneider, S. E., & Posson-Brown, J. 2002, in preparation.
Salucci, P. & Persic, M. 1999, MNRAS, 309, 923.
Shostak, G. S. 1987, A&A, 175, 4 Skillman, E. D., Bothun, G. D., Murray, M. A., & Warmels, R. H. 1987, A&A, 185, 61.
Steidel, C. C., Pettini, M., Dickinson, M., & Persson, S. E. 1994, AJ, 108, 2046.
Storrie-Lombardi, L. J. & Wolfe, A. M. 2000, ApJ, 543, 552.
Tacconi, L. J., & Young, J. S., 1986, ApJ, 308, 600.
Taylor, C. L., Brinks, E., Pogge, R. W., & Skillman, E. D. 1994, AJ, 107, 971.
Tonry, J. L., Blakeslee, J. P., Ajhar, E. A., & Dressler, A. 2000, ApJ, 530, 625.
van Driel, W., Balkowski, C., & van Woerden, H. 1989, A&A, 218, 49.
van Driel, W., & van Woerden, H. 1989, A&A, 225, 317.
van Driel, W., Rots, A. H., & van Woerden, H. 1988, A&A, 204, 39.
van Woerden, H., van Driel, W., Braun, R., & Rots, A. H. 1993, A&A, 269, 15.
van Zee, L., Haynes, M. P., Salzer, J. J., & Broeils, A. H. 1996, AJ, 112, 129.
van Zee, L., Haynes, M. P., Salzer, J. J., & Broeils, A. H. 1997, AJ, 113, 1618.
van Zee, L., Skillman, E. D., & Salzer, J. J. 1998, AJ, 116, 1186.
Verheijen, M. A. W. & Sancisi, R. 2001, A & A, 370, 765.
Walter, F., & Brinks, E. 2001, AJ, 121, 3026.
Wevers, B. M. H. R., van der Kruit, P. C., & Allen, R. J., 1986, A&AS, 66, 505.
Wilding, T., Alexander, P., & Green, D. A. 1993, MNRAS, 263, 1075.
Wolfe, A. M. & Prochaska, J. X. 2000, ApJ, 545, 603.
Wolfe, A. M. 1995, in QSO Absorption Lines, ed. G. Meylan (Heidelberg: Springer), 13.
Wolfe, A. M., Lanzetta, K. M., Foltz, C. B., & Chaffee, F. H. 1995, ApJ, 454, 698.
Young, L. M., & Lo, K. Y. 1996, ApJ, 462, 203.
Young, L. M., & Lo, K. Y. 1997, ApJ, 490, 710.
Zwaan, M., Briggs, F., & Verheijen, M. 2001, in Extragalactic Gas at Low Redshift, ed. J. S. Mulchaey & J. Stocke (San Francisco: ASP), 254, 169.
Zwaan, M., Briggs, F. H., Sprayberry, D. & Sorar, E. 1997, ApJ, 490, 173.